Macrophage $P2Y_6$ Receptor Signaling Selectively Activates NFATC2 and Suppresses Allergic Lung Inflammation

Jun Nagai,*,† Junrui Lin,† and Joshua A. Boyce*,†,‡,§

Innate immune responses to innocuous Ags can either prevent or facilitate adaptive type 2 allergic inflammation, but the mechanisms are incompletely understood. We now demonstrate that macrophage UDP-specific type 6 purinergic ($P2Y_6$) receptors selectively activate NFATC2, a member of the NFAT family, to drive an innate IL-12/IFN-γ axis that prevents type 2 allergic inflammation. UDP priming potentiated IL-12p40 production in bone marrow–derived macrophages (BMMs) stimulated by the house dust mite *Dermatophagoides farinae* (Df) in a $P2Y_6$-dependent manner. Inhibitions of phospholipase C, calcium increase, and calcineurin eliminated UDP-potentiated Df-induced IL-12p40 production. UDP specifically induced nuclear translocation of NFATC2, but not NFATC1 and NFATC3, in BMMs in a $P2Y_6$-dependent manner. UDP-potentiated IL-12p40 production by BMMs and Df-induced IL-12p40 gene expression by alveolar macrophages were abrogated in cells from *Nfatc2* knockout mice. Pulmonary transplantation of wild-type but not *Nfatc2* knockout macrophages increased Df-induced IL-12 production and IFN-γ expression in $P2ry6^{fl/fl/Cre/+}$ recipient mice. Finally, *Nfatc2* knockout mice showed significantly increased indices of type 2 immunopathology in response to Df challenge, similar to $P2ry6^{fl/fl/Cre/+}$ mice. Thus, macrophage $P2Y_6$ receptor signaling selectively utilizes NFATC2 to potentiate an innate IL-12/IFN-γ axis, a potential mechanism that protects against inappropriate type 2 immune responses. ***The Journal of Immunology*, 2022, 209: 2293–2303.**

Innate immune responses initiate both host defense against pathogens and immune responses to innocuous environmental Ags (1). Pathogens and Ags elicit cytokine production by tissue-resident cells that engulf (and/or are activated by) the pathogen or Ag, and they bridge to the subsequent adaptive immune response (2). Innate immune responses against helminthic parasites and certain protease Ags elicit adaptive type 2 inflammation (T2I) involving tissue infiltration by eosinophils (3). When directed against innocuous environmental Ags, the resultant T2I results in common respiratory diseases such as asthma and allergic rhinitis. Pathogen-associated molecular patterns, such as endotoxin, and endogenously generated danger-associated molecular patterns (DAMPs) signal to specific receptors on cells of the immune system to control the magnitude of innate immune response and the nature of the subsequent adaptive immune response (1, 4). The hygiene hypothesis proposes that decreased exposure to microbial products is one of the main drivers of allergic airway disease (5, 6). Supporting this idea, exposure to LPS before or during sensitization protects mice from developing experimental house dust mite–induced asthma (7, 8). These studies suggest regulation of the initial innate immune response can control the subsequent T2I.

Alveolar macrophages are among the essential first lines of defense against pollutants and pathogens that initiate an innate immune response (9). They engulf and process foreign invaders to the lung tissue and have the capacity to both induce and prevent inflammatory responses to maintain tissue homeostasis (10). In an animal model of asthma, depletion of alveolar macrophages or lack of transcriptional factor IFN regulatory factor 5 (IRF5) in alveolar macrophage results in enhanced T2I, suggesting that alveolar macrophages can have protective roles in this context (11, 12). However, the driving forces and regulatory mechanisms of alveolar macrophage responses to Ags are incompletely understood.

In addition to their roles as subunits of nucleic acids and vehicles of energy transfer intracellularly, released nucleotides can also serve as DAMPs (13). Nucleotides are released from tissue-resident cells or recruited myeloid cells following stimulation, facilitating rapid cell–cell communication (14, 15). Extracellular nucleotides signal through purinergic (P2) receptors that include G protein–coupled receptors (GPCRs) (P2Y receptors: $P2Y_{1,2,4,6,11-14}$) and ion channels (P2X receptors: $P2X_{1-7}$) with specificities for respective nucleotide species (ATP, ADP, UTP, UDP) (16). Importantly, P2Y receptor blockade is a potential off-target effect of competitive antagonists of the type 1 receptor for cysteinyl leukotrienes ($CysLT_1$), which block several P2Y receptors at 0.5–1.5 μM, consistent with maximal serum concentrations achieved after a single oral dose in human subjects (17–20). Allergen challenge causes rapid accumulation of ATP in the airways of asthmatic subjects and mice with experimentally induced asthma (21). ATP primes lung dendritic cells to promote

*Department of Medicine, Harvard Medical School, Boston, MA; †Division of Allergy and Clinical Immunology, Brigham and Women's Hospital, Boston, MA; ‡Department of Pediatrics, Harvard Medical School, Boston, MA; and §Jeff and Penny Vinik Center for Allergic Disease Research, Boston, MA

ORCIDs: 0000-0003-4720-5065 (J.N.); 0000-0002-2401-2351 (J.A.B.).

Received for publication June 27, 2022. Accepted for publication October 5, 2022.

This work was supported by contributions from the Vinik Family Foundation, the Kaye Family Foundation, National Institute of Allergy and Infectious Diseases Grants R21AI156068, AI078908, R37AI052353, R01AI136041, R01AI130109, U19AI095219, and by National Heart, Lung, and Blood Institute Grants HL111113, HL117945, and R01HL136209.

J.N. designed and performed the experiments and analyzed the data; J.L. provided technical assistance; and J.A.B. oversaw the project and experiments and composed the manuscript with J.N.

Address correspondence and reprint requests to Dr. Jun Nagai, Division of Allergy and Clinical Immunology, Department of Medicine, Brigham and Women's Hospital, Hale Building for Transformative Medicine, 60 Fenwood Road, Room 5006, Boston, MA 02115. E-mail address: jnagai@partners.org

The online version of this article contains supplemental material.

Abbreviations used in this article: +/+, $P2ry6^{fl/fl/+/+}$; BAL, bronchoalveolar lavage; BM, bone marrow; DAMP, danger-associated molecular pattern; Df, *Dermatophagoides farinae*; GPCR, G protein–coupled receptor; PLC, phospholipase C; qPCR, quantitative PCR; T2I, type 2 inflammation; WT, wild-type.

T2I to the innocuous experimental Ag OVA and acts at $P2Y_2$ receptors on respiratory epithelial cells to induce the release of IL-33, a T2I-promoting DAMP (21–23). ATP also activates mast cells through $P2X_7$ ion channels, resulting in degranulation and amplification of IL-33–induced productions of proinflammatory cytokines and lipid mediators (24–26). ADP induces the nuclear-to-cytoplasmic translocation and subsequent release of IL-33 by human airway epithelial cells through $P2Y_{13}$ (27). Thus, the purine nucleotides ATP and ADP facilitate T2I through several mechanisms and targets.

Among immune cells, macrophages express an especially diverse array of P2 receptors, suggesting the potential for a wide range of nucleotide-induced functional responses. Human alveolar macrophages express the P2Y ($P2Y_1$, $P2Y_2$, $P2Y_4$, $P2Y_6$, $P2Y_{11}$, $P2Y_{12}$, and $P2Y_{14}$) and P2X families ($P2X_1$, $P2X_4$, $P2X_5$, and $P2\times_7$), similar to mouse macrophages (28). ATP increases secretion of the cytokines IL-6 and IL-1β by human alveolar macrophages while suppressing IL-12p40 production through $P2X_7$, $P2Y_1$, or $P2Y_2$ (28). Macrophages also express especially high levels of $P2Y_6$ receptors, which specifically recognize the pyrimidine nucleotide UDP at nanomolar concentrations. $P2Y_6$ receptor signaling can inhibit T2I-mediated lung inflammation by enhancing the initial innate immune response (29–31). In the absence of $P2Y_6$ receptors, alveolar macrophages show diminished IL-12 production and Th1-associated chemokines that drive the accumulation of IFN-γ–generating NK cells during the early sensitization phase of airway disease caused by repetitive inhalation of an extract from the house dust mite *Dermatophagoides farinae* (Df) (30). As a result, $P2ry6^{fl/fl/Cre/+}$ mice display exacerbated T2I-mediated inflammation in this model. Although all P2Y receptors signal principally through Gα proteins, the mechanisms through which $P2Y_6$ receptors specifically facilitate IL-12 production and enhance the innate immune response are still unknown. In this study, we demonstrate that $P2Y_6$ signaling results in the selective nuclear translocation of NFATC2, a member of the NFAT family. Deletion of NFATC2 in macrophages attenuates UDP/$P2Y_6$-potentiated innate immunity through the IL-12p40 pathway. These data reveal a specialized novel mechanism by which UDP/$P2Y_6$ signaling potentiates the innate alveolar macrophage response to innocuous Ags and modifies the subsequent adaptive immune response and resultant T2I.

Materials and Methods

Mice

C57BL/6 mice were purchased from The Jackson Laboratory and Charles River Laboratories. $P2ry6^{fl/fl/+/+}$ (+/+) mice and $P2ry6^{fl/fl/Cre/+}$ mice were generated as previously reported and backcrossed for 10 generations with C57BL/6 mice (29). To delete the $P2Y_6$ receptor, we used the ubiquitous inducible Rosa26 Cre recombinase in 8- to 16-wk-old $P2ry6^{fl/fl/Cre/+}$ mice by daily i.p. injections of tamoxifen (1 mg; MilliporeSigma) for 5 d, beginning 14 d before the first Df treatment, or bone marrow (BM) harvesting. $Nfatc1^{fl/fl}$ mice (32) were provided by Antonios O. Aliprantis and intercrossed with *CX3CR1-Cre* mice (The Jackson Laboratory, stock no. 025524) (33) to generate $Nfatc1^{fl/fl/CX3CR1Cre/+}$ mice. $Nfatc2^{-/-}$ mice were provided by Anjana Rao and Patrick Hogan (La Jolla Institute, La Jolla, CA) (34). All mice were housed in groups of two to five mice per cage with a standard 12-h light/12-h dark cycle and provided food and water ad libitum. All experiments were in accordance with review and approval by the Animal Care and Use Committee of Brigham and Women's Hospital.

BM-derived macrophage generation

BM-derived macrophages (BMMs) were generated as described (30). BM cells were obtained from wild-type (WT), $Nfatc2^{-/-}$, or tamoxifen-treated $P2ry6^{fl/fl/Cre/+}$ mice and cultured in DMEM/F12 medium supplemented with 10% heat-inactivated FBS, 100 U/ml penicillin, 100 μg/ml streptomycin, 2 mM L-glutamine, and 100 ng/ml recombinant mouse M-CSF (R&D Systems). On day 3, 5 ml of complete medium was added, and the adherent cells were harvested on day 5 or 6.

Induction of allergic inflammation

Allergic inflammation was induced by separate intranasal sensitization (20 μg on days 0 and 1) and challenge (3 μg on days 14 and 15) with Df, as described previously (30). Mice were euthanized on day 0 (6 h), 2, or 16, and lungs were lavaged twice with 1.0 ml of PBS containing 0.5 mM EDTA. Bronchoalveolar lavage (BAL) fluid cells were cytocentrifuged onto slides, stained with Diff-Quik (Siemens Healthcare Diagnostics), and differentially counted.

ELISA analysis

The concentration of IL-12p40 in supernatants from the ex vivo BMMs was measured by using commercially available ELISA (BD Biosciences) kits according to the instructions of the manufacturer. Concentrations of BAL fluids IL-4, IL-5, IL-13, and serum IgE were assayed by using commercially available ELISA kits from Thermo Fisher Scientific.

Real-time quantitative PCR of mRNA transcripts

BAL cells were collected at the time of euthanasia. Alveolar macrophages were purified from BAL of Df-treated WT and $Nfatc2^{-/-}$ mice by positive CD11c MACS selection (Miltenyi Biotec), according to the manufacturer's protocol. Alveolar macrophage purity was checked by staining with Diff-Quik and was confirmed to be >95%. Total RNA was isolated from alveolar macrophages and BMMs with QIAzol reagent (Qiagen). For alveolar macrophages, glycogen (RNA grade, Thermo Fisher Scientific) was used as an inert carrier to increase nucleic acid recovery from alcohol precipitation. Total RNA was converted to cDNA using an RT^2 first-strand kit (Qiagen) consisting of oligo(dT) primers and random hexamers. The expression of each gene was examined using an RT^2 SYBR Green quantitative PCR (qPCR) master mix (Qiagen). All qPCR primer efficiencies were validated based on a standard curve for each gene. Expression levels of transcripts were normalized to the expression of *Gapdh*. All primer sequences are listed in Supplemental Table.

Confocal microscopy

For confocal microscopy of the BMMs and alveolar macrophages, cells were washed and immediately fixed/permeabilized with a BD Cytofix/Cytoperm kit (BD Biosciences). Primary mouse anti-NFATC1, mouse anti-NFATC2, mouse anti-NFATC3, and rabbit anti-Iba1 were added to the TBS-based blocking buffer containing 0.1% Triton X-100 and 1% BSA for incubation overnight. After washing three times with TBS containing 0.1% Triton X-100, the cells were incubated with Alexa Fluor 555 donkey anti-mouse secondary Ab and Alexa Fluor 488 donkey anti-rabbit secondary for 3 h. After washing three times with TBST, the slides were mounted with Fluoroshield mounting medium with DAPI. Images were acquired at the Brigham and Women's Hospital Confocal Microscopy Core Facility using the Zeiss LSM 800 with Airyscan confocal system on a Zeiss Axio Observer Z1 inverted microscope with a ×63 Zeiss oil (1.4 numerical aperture) objective.

Pulmonary macrophage transplantation

Pulmonary macrophage transplantation was performed as described previously (30, 35). BM cells obtained from WT and $Nfatc2^{-/-}$ mice were harvested, and this suspension (~27×10^6 cells/10 ml) was cultured in DMEM medium supplemented with 10% heat-inactivated FBS, 100 U/ml penicillin, 100 μg/ml streptomycin, 2 mM L-glutamine, and 10 ng/ml recombinant mouse GM-CSF and 5 ng/ml recombinant mouse M-CSF (both from R&D Systems). The next day, nonadherent and weakly adherent cells were transferred to a new petri dish and cultured. After 2 d, 10 ml of medium with GM-CSF and M-CSF was exchanged from each plate, and 5 d after seeding, adherent BMMs were used for alveolar macrophage transplantation. Two million BMMs in a total volume of 50 μl of PBS were administered into the lungs of +/+ mice using a relatively noninvasive endotracheal instillation method described previously (35). The next day, mice were administered with tamoxifen for 5 consecutive days, and 10 d after the last tamoxifen treatment, allergic pulmonary inflammation was induced by intranasal instillation of Df.

Calcium flux assay

We developed 1321N1 cells stably expressing mouse $P2Y_6$ 1321N1 cells previously (30). The cell suspension was plated in a 384-well plate (Greiner Bio-One) at a density of 1×10^4 cells/well. Following incubation for 18–24 h, cells were changed to fresh HBSS medium and loaded with Fluo-8 (final, 2 μM; AAT Bioquest), probenecid (final, 2.5 mM; Thermo Fisher Scientific), and PowerLoad (Thermo Fisher Scientific) in HBSS. After 30 min, respective inhibitors (YM-254890, U73122, BAPTA-AM) and UDP (MilliporeSigma) were added at defined concentrations, followed by an immediate recording of the fluorescence using a functional drug screening system/FDSS7000EX (Hamamatsu). Fluorescence intensity was expressed as a Fluo-8 ratio (tested value/basal value).

Reagents

All key reagent sources are listed in Supplemental Table.

Statistical analysis

All values are presented as mean ± SEM. Statistical analysis was performed using GraphPad Prism 9 (GraphPad Software). When comparing two groups, a paired *t* test or Mann–Whitney *U* test was used based on the sample distribution. Differences among multiple groups were assessed using one-way ANOVA with a Tukey's or Dunnett's multiple comparison test or two-way ANOVA followed by a Bonferroni's multiple comparison test. A p value <0.05 was considered statistically significant.

Results

UDP priming potentiates the Df-induced IL-12 production through $P2Y_6$/Gαq/phospholipase C/Ca^{2+} influx

To determine how UDP/$P2Y_6$ receptor signaling regulates innate immune responses by macrophages, we measured IL-12p40, a subunit of both the Th1-promoting cytokine IL-12 and the Th17-promoting cytokine IL-23, in the supernatant of BM-derived macrophages (BMMs) from +/+ and *P2ry6*$^{fl/fl/Cre/+}$ mice. UDP alone did not increase the secretion of IL-12p40 from +/+ and *P2ry6*$^{fl/fl/Cre/+}$ BMMs (data not shown), and it did not potentiate Df-induced production of IL-12p40 when administered simultaneously with Ag (Fig. 1A). However, pretreatment of BMMs with UDP potentiated Df-induced secretion of IL-12p40 by +/+ BMMs, reaching a peak 0.5–3 h after UDP priming and declining thereafter. These UDP priming effects were abolished in BMMs from *P2ry6*$^{fl/fl/Cre/+}$ mice. We next assessed the dose-dependent ability of four nucleotides (UDP, UTP, ATP, ADP) to alter Df-induced IL-12p40 production. UDP priming dose-dependently increased Df-induced IL-12p40 production that was absent in BMMs from *P2ry6*$^{fl/fl/Cre/+}$ mice (Fig. 1B). High concentrations of UTP resulted in a modest but significant upregulation of IL-12p40 production by +/+, but not *P2ry6*$^{fl/fl/Cre/+}$, BMMs. ATP and ADP failed to potentiate the Df-induced IL-12p40 production.

The functions of GPCRs are mediated principally by their coupling to Gα proteins (Gαs, Gαi, Gαq, and Gα12/13 proteins) (16, 36). To determine the specific Gα proteins responsible for the downstream signaling pathways of the $P2Y_6$ receptor for potentiation of macrophage IL-12p40 production, we treated the cells with selective pharmacological inhibitors of Gα proteins. A specific inhibitor of Gαq, YM-254890 (37), significantly inhibited the UDP-potentiated IL-12p40 production in a dose-dependent manner, without affecting IL-12p40 production induced by Df alone (Fig. 2A). YM-254890 blocked UDP-induced Ca^{2+} influx in mouse $P2Y_6$-expressing 1321N1 cells, albeit at higher doses than were needed to block UDP-elicited potentiation of IL-12p40 production by BMMs. In contrast, the Gαi inhibitor pertussis toxin and pharmacological inhibition of Rho, a downstream target of Gα12/13 proteins, increased the IL-12p40 production even in the absence of UDP priming. As $P2Y_6$/Gαq signaling induces phospholipase C (PLC) activation and subsequent increases of intracellular calcium, we examined the effects of a PLC inhibitor (U73122) and an intracellular calcium chelator (BAPTA-AM) on UDP-potentiated IL-12p40 production in BMMs (Fig. 2B). Consistent with a role for $P2Y_6$-initiated Gαq signaling, U73122 (1 μM) and BAPTA-AM (3 μM) significantly reduced UDP-potentiated IL-12p40 production. These same inhibitors blocked UDP-induced calcium influx in mouse $P2Y_6$-expressing 1321N1 cells and BMMs, albeit higher doses were needed to completely block UDP-elicited calcium flux (Fig. 2B, Supplemental Fig. 1).

Nuclear translocation of NFATC2 mediates UDP-potentiated IL-12 production by macrophages

We next sought to identify transcription factors mediating the UDP priming event. Calcium entry often induces transcriptional activation of both NF-κB as well as NFAT (38, 39). NF-κB is well known to drive cytokine expression by macrophages (40). Df activates NF-κB through the C-like lectin receptor dectin 2 and the signaling adaptor CARD9 (41, 42). The NF-κB nuclear translocation inhibitor JSH-23 blocked Df-induced IL-12p40 production with or without UDP priming (Fig. 3A). We hypothesized that NFAT, which is activated by intracellular calcium increase and calcineurin (a calcium-dependent phosphatase), might provide a second signal by which UDP/$P2Y_6$ could augment Df-elicited NF-κB–mediated transcriptional activation in BMMs. The UDP priming effect was efficiently blocked in the presence of calcineurin inhibitors FK506 and cyclosporin A, without affecting Df-induced IL-12p40 production (Fig. 3B).

Of the five known isoforms of NFAT, BMMs dominantly expressed *Nfatc1*, *Nfatc2*, and *Nfatc3* mRNAs (Supplemental Fig. 2A). We therefore focused our subsequent analyses on these three isoforms. Notably, Df treatment of +/+ BMMs for 6 h decreased their expressions of all three dominant *Nfat* isoforms, as well as *P2ry6* transcripts (Supplemental Fig. 2B).

To determine the time course of UDP-induced NFAT activation, we performed immunofluorescence staining of BMMs stimulated with UDP. NFATC2 translocated from cytosol to the nucleus as early as 10 min after UDP priming and decreased thereafter (Fig. 4A). In contrast, UDP did not elicit nuclear translocation of NFATC1 or NFATC3. Stimulation of BMMs with calcium ionophore induced nuclear translocation of both NFATC1 and NFATC2 but not NFATC3 (Fig. 4B). BMMs from *P2ry6*$^{fl/fl/Cre/+}$ mice showed diminished UDP-induced NFATC2 nuclear translocation, whereas ionomycin-induced NFATC1 and NFATC2 activation were unaffected by the absence of $P2Y_6$. Both NFAT inhibitors FK506 and cyclosporin A blocked the UDP-elicited NFATC2 nuclear translocation at the same dose that inhibited IL-12p40 production (Fig. 4C).

To confirm the involvement of NFATC2 in UDP-potentiated IL-12p40 production, we used BMMs from *Nfatc2*$^{-/-}$ mice. As predicted, UDP failed to potentiate IL-12p40 production in *Nfatc2*$^{-/-}$ BMMs, and it failed to potentiate their expression of *Il12b* transcript (Fig. 5A). Priming of WT BMMs with UDP also potentiated their Df-induced expressions of mRNAs encoding the chemokine CCL5 and the cytokine CSF2. This potentiation was absent in both *Nfatc2*$^{-/-}$ and *P2ry6*$^{fl/fl/Cre/+}$ BMMs (Fig. 5). To determine whether $P2Y_6$ receptor signaling through NFATC2 regulated IL-12 production by alveolar macrophages, we measured *Il12b* transcripts in alveolar macrophages harvested from BAL fluid. To determine the time course of Df-induced *Il12b* upregulation, we performed qPCR of alveolar macrophages stimulated with Df. Df-induced *Il12b* transcripts reached a peak at 6 h after Df stimulation and decreased thereafter (Supplemental Fig. 3A). In contrast to BMMs, exogenous UDP failed to potentiate Df-induced *Il12b* transcripts (data not shown). However, Df-induced *IL12b* upregulation was diminished in BMMs from *P2ry6*$^{fl/fl/Cre/+}$ mice (Fig. 6A). This Df-induced *IL12b* upregulation (which involves an endogenous UDP potentiation effect) was also abolished in alveolar macrophages from *Nfatc2*$^{-/-}$ mice, but not from *Nfatc1*$^{-/-}$ mice. Each of the gene deletions in respective knockout mice was confirmed by qPCR of alveolar macrophages (Fig. 6B).

Adoptively transferred BMMs from WT, but not Nfatc2$^{-/-}$ *mice, restores both early innate IL-12 production and subsequent IFN-γ production in* P2ry6$^{-/-}$ *recipient mice.*

To confirm that NFATC2 is necessary for UDP/$P2Y_6$ receptor–potentiated IL-12 production by alveolar macrophages, we used an established pulmonary macrophage transplantation protocol that permits engraftment by BMMs without myeloablation (35). BMMs derived from WT and *Nfatc2*$^{-/-}$ mice were delivered intratracheally

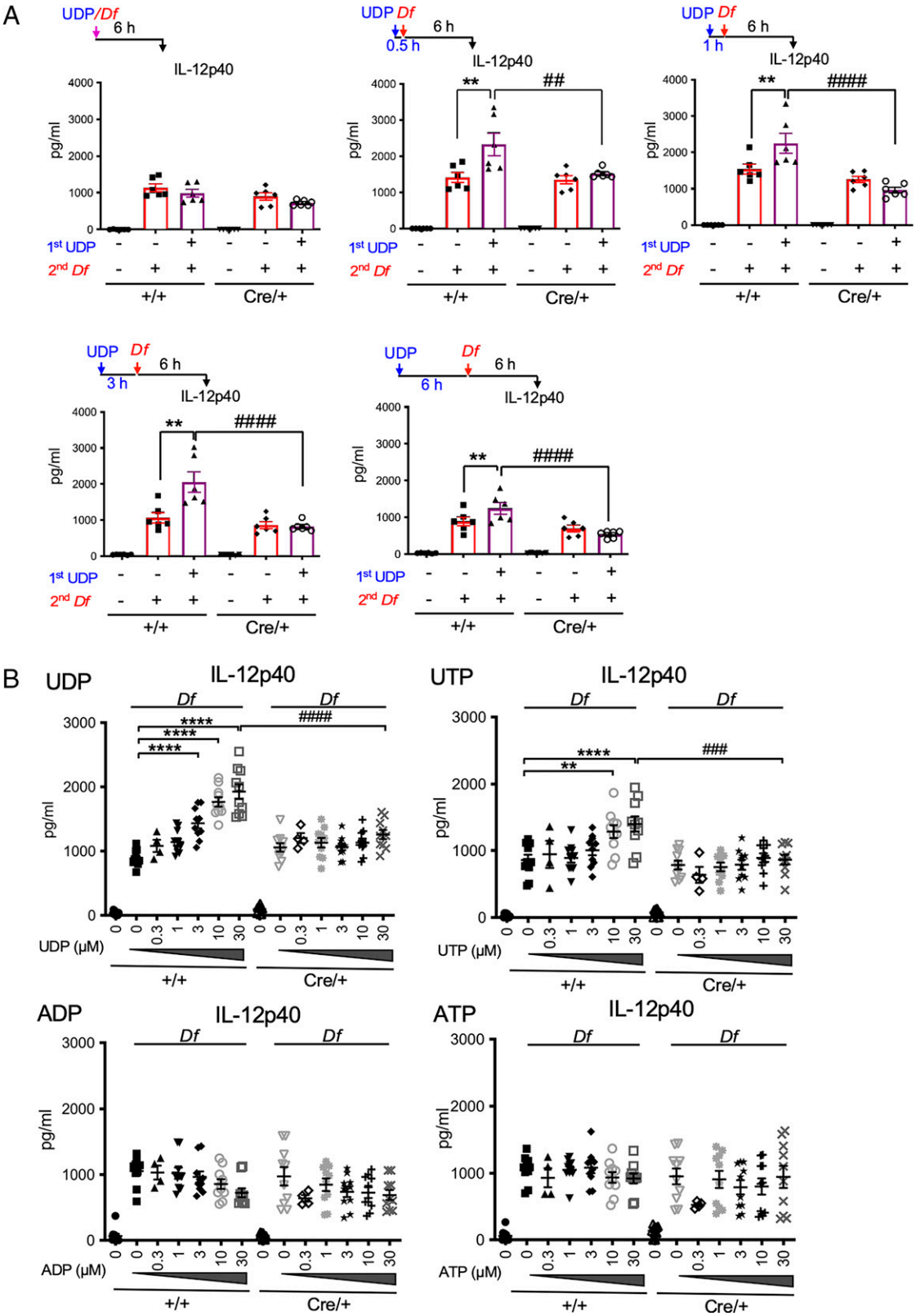

FIGURE 1. Priming with UDP potentiates Df-induced IL-12 production in BMMs. (**A**) BMMs from *P2ry6*$^{fl/fl/+/+}$ (+/+) and *P2ry6*$^{fl/fl/Cre/+}$ (Cre/+) mice were treated with Df (100 μg/ml) for 6 h after priming with UDP (30 μM) for periods of 0, 0.5, 1, 3, and 6 h. IL-12p40 in supernatants was quantified by ELISA (n = 6 from 6 mice). The results are from one experiment. The data for periods of 0 and 1 h were replicated in additional experiments. Values are means ± SEM. $^{**}p < 0.01$ versus vehicle treatment, by paired t test; $^{\#\#}p < 0.01$, $^{\#\#\#\#}p < 0.0001$ versus +/+ mice, by one-way ANOVA followed by a Tukey's multiple comparison test. (**B**) Dose-dependent effects of UDP, UTP, ATP, and ADP (n = 10 from 10 mice, two experiments, except for 0.3 μM nucleotides with n = 4 from 4 mice) for 1 h followed by Df (100 μg/ml) for 6 h, measured IL-12p40 ELISA. Values are means ± SEM. $^{**}p < 0.01$, $^{****}p < 0.0001$ versus vehicle treatment, by Dunnett's multiple comparison test; $^{\#\#\#}p < 0.001$, $^{\#\#\#\#}p < 0.0001$ versus +/+ mice, by one-way ANOVA followed by Tukey's multiple comparison test.

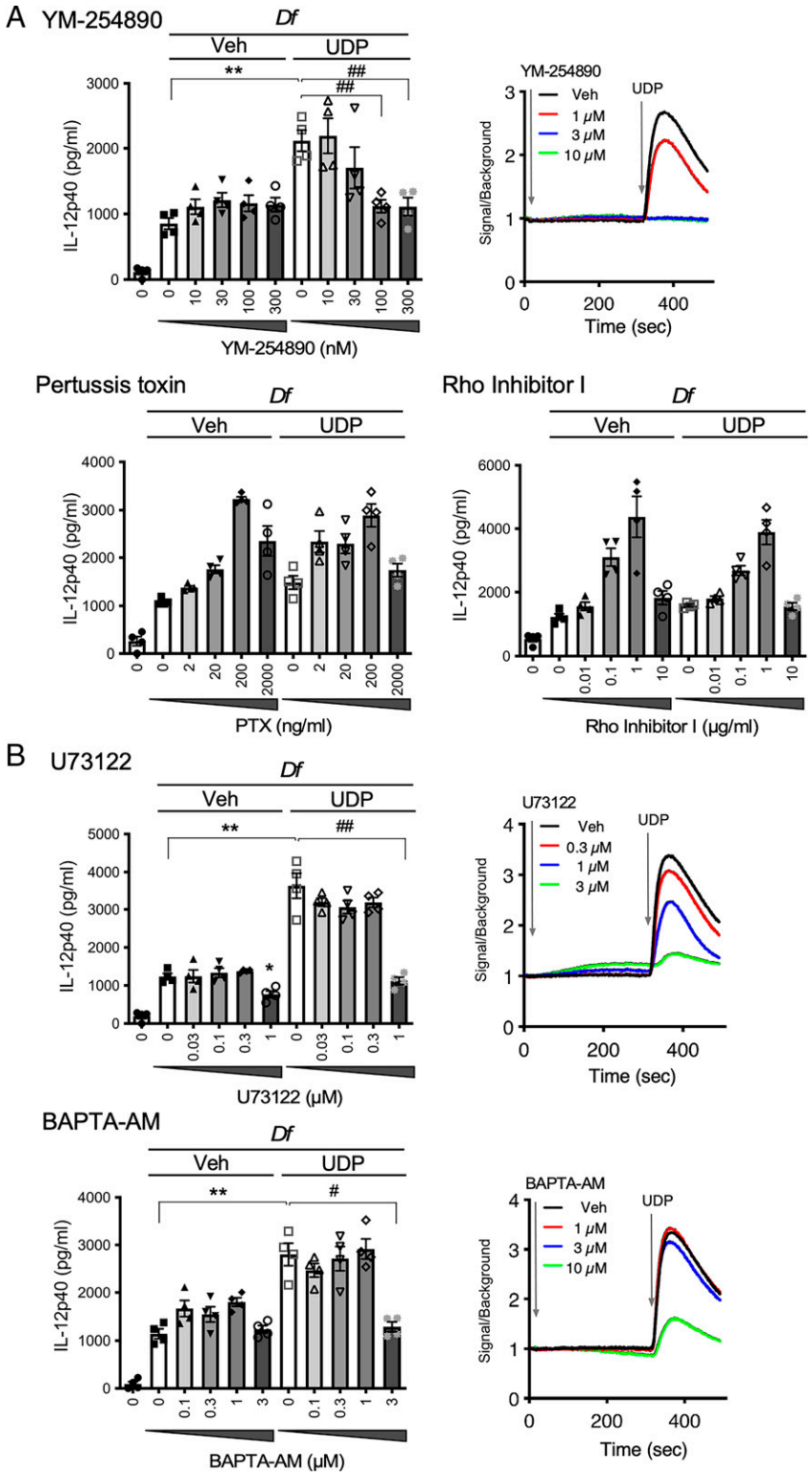

FIGURE 2. $P2Y_6$ signaling potentiates Df-induced IL-12 production through Gαq/PLC/Ca^{2+} influx in BMMs. (**A**) Dose-dependent effects of Gαq (YM-254890), Gαi (pertussis toxin), and Gα12/13-Rho (Rho inhibitor I) inhibitors pretreatment on Df-induced IL-12p40 production with or without UDP priming (30 μM, $n = 4$ from 4 mice). The results are from one experiment. The data for 100 nM YM-254890, 200 ng/ml pertussis toxin, and 1 μg/ml Rho inhibitor I were replicated in an additional experiment. The BMMs were treated with pertussis toxin and Rho inhibitor I for 16 h or Y27632 for 30 min and stimulated with or without UDP for 1 h and Df for 6 h. Values are means ± SEM. $^{**}p < 0.01$ versus vehicle treatment, by paired *t* test; $^{\#\#}p < 0.01$ versus vehicle treatment, by Dunnett's multiple comparison test. YM-254890 blocked UDP-elicited calcium flux induced in 1321N1 cells stably expressing mouse P2ry6 ($n = 3$, upper right panel). (**B**) Effects of PLC inhibitor (U73122) and cell-permeant chelator (BAPTA-AM) on Df-induced IL-12p40 production with or without UDP priming for 1 h (30 μM, $n = 4$ from 4 mice). The BMMs were pretreated with U73122 or BAPTA-AM for 30 min. The results are from one experiment. The data for 1 μM U73122 and 3 μM BAPTA-AM were replicated in an additional experiment. Values are means ± SEM. $^{**}p < 0.01$ versus vehicle treatment, by paired *t* test; $^{\#}p < 0.05$, $^{\#\#}p < 0.01$ versus vehicle treatment, by Dunnett's multiple comparison test. U73122 and BAPTA-AM blocked UDP-elicited calcium flux induced in 1321N1 cells stably expressing mouse P2ry6 ($n = 3$, right panel). Representative calcium flux data from two experiments are shown.

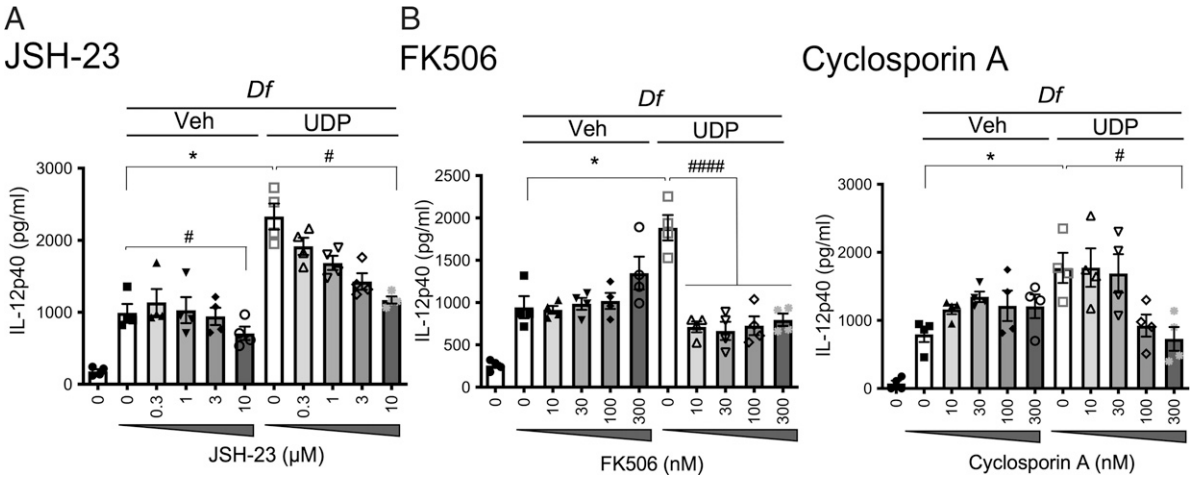

FIGURE 3. NFAT inhibitors selectively inhibit the UDP-elicited potentiation of Df-induced IL-12 production in BMMs. (**A**) Effect of the NF-κB nuclear translocation inhibitor JSH-23 on Df-induced IL-12p40 production with or without UDP priming for 1 h ($n = 4$ from 4 mice). (**B**) Effects of calcineurin inhibitors FK506 and cyclosporin A specifically blocked the UDP-elicited potentiation of Df-induced IL-12 production ($n = 4$ from 4 mice). The results are from one experiment. The data for 10 μM JSH-23 and 100–300 nM FK506 and cyclosporin A were replicated in an additional experiment. Values are means ± SEM. $^{*}p < 0.05$ versus vehicle treatment, by paired t test or Mann–Whitney U test based on the sample distribution; $^{\#}p < 0.05$, $^{\#\#\#\#}p < 0.0001$ versus vehicle treatment, by Dunnett's multiple comparison test.

to recipient *P2ry6*$^{fl/fl/Cre/+}$ mice. The engrafted mice were sensitized with Df on day 0 and 1, and quantities of IL-12p40 were measured on day 2 (Fig. 7A). *P2ry6* transcript in *P2ry6*$^{fl/fl/Cre/+}$ recipient mice engrafted with WT and *Nfatc2*$^{-/-}$ BMMs confirmed the presence of the transferred macrophages for >17 d (Fig. 7B). Df-treated *P2ry6*$^{fl/fl/Cre/+}$ recipient mice engrafted with WT BMMs showed markedly increased levels of IL-12p40 in the BAL fluid compared with *P2ry6*$^{fl/fl/Cre/+}$ recipient mice engrafted with *Nfatc2*$^{-/-}$ BMMs after two sensitizing doses of Df (Fig. 7C). Additionally, recipients of WT BMMs, but not recipients of *Nfatc2*$^{-/-}$ BMMs, showed increased IFN-γ transcripts by BAL fluid cells (Fig. 7D). IL-12p40 levels and IFN-γ transcripts were tightly correlated (Fig. 7E).

Absence of NFATC2 amplifies lung T2I in response to Df

To determine whether NFATC2 activation was essential to enforce the innate immune responses and suppress T2I with Df sensitization and subsequent challenges, we sensitized *Nfatc2*$^{-/-}$ mice and WT controls with Df on day 0 and 1 and compared their T2I with subsequent Df challenges on day 14 and 15 (Fig. 8A). qPCR of alveolar macrophages (CD11c^{+} BAL fluid cells) sorted Df-treated *Nfatc2*$^{-/-}$ mice by 6 h after the first sensitization with Df demonstrated a significant

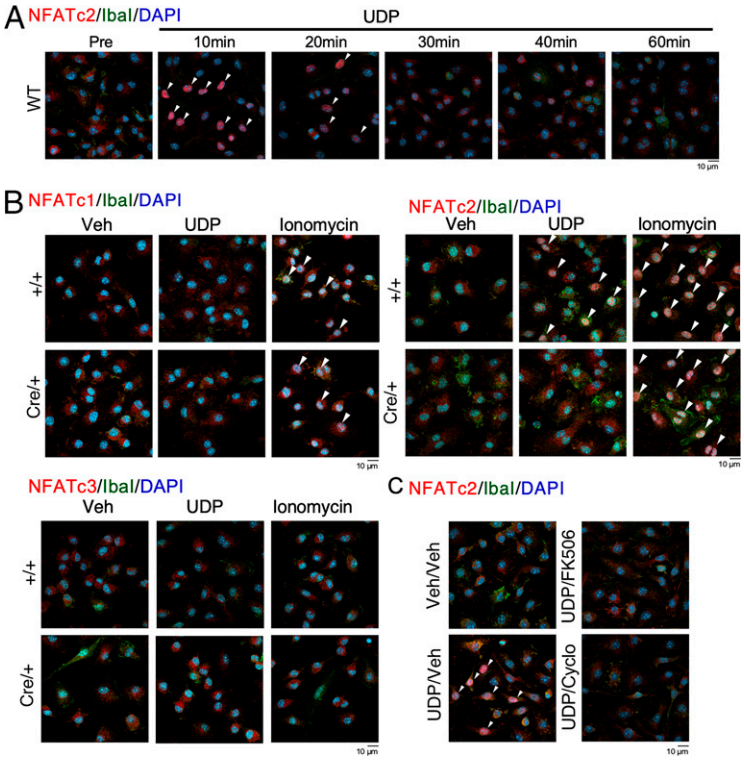

FIGURE 4. UDP selectively induces nuclear translocation of NFATC2, but not NFATC1 and NFATC3, in BMMs. (**A**) Time course of nuclear NFATC2 translocation in WT BMMs. BMMs from WT mice were treated with UDP (100 μM) for the indicated time intervals. Cells were stained with anti-NFATC2 and anti-Iba1 Abs (macrophage marker) and visualized with Alexa Fluor 555 (red)– and Alexa Fluor 488 (green)– conjugated secondary Abs with nuclei stain DAPI (blue). Arrowheads indicate nuclear localization of NFATC2. Representative images from four mice (one experiment) are shown using the Zeiss LSM 800 with an Airyscan confocal system on a Zeiss Axio Observer Z1 inverted microscope with a ×63 Zeiss oil (1.4 numerical aperture) objective. The data for 10 min were replicated in an additional experiment. (**B**) BMMs from +/+ and *P2ry6*$^{fl/fl/Cre/+}$ (Cre/+) mice were treated with 100 μM UDP or 10 μM ionomycin for 10 min. Cells were stained with anti-NFATC1/2/3 and anti-Iba1 Abs and visualized with Alexa Fluor 555 (red)– and Alexa Fluor 488 (green)–conjugated secondary Abs with nuclei stain DAPI (blue). Representative images from two experiments ($n = 8$ from 8 mice) are shown. (**C**) Calcineurin inhibitor FK506 (10 nM) and cyclosporin A (300 nM) blocked the UDP-induced nuclear translocation of NFATC2. Representative images from four mice (one experiment) are shown. Scale bars, 10 μm.

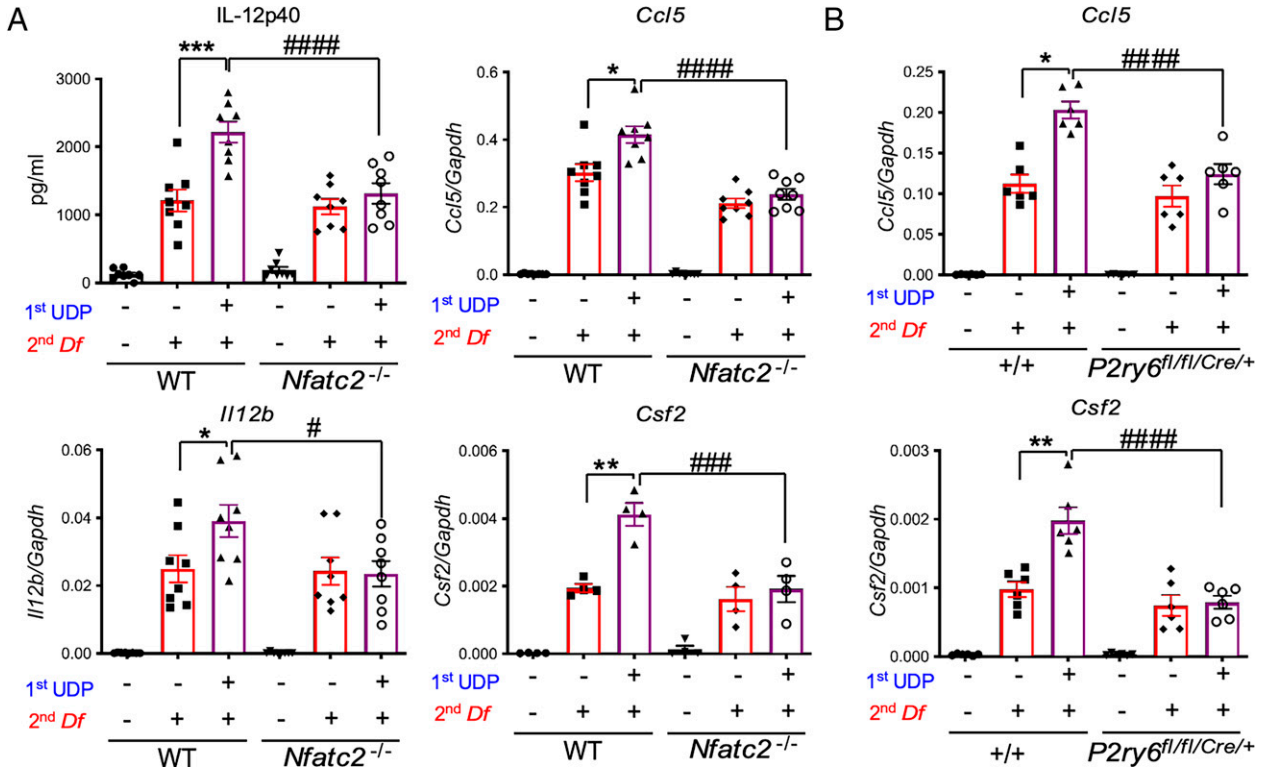

FIGURE 5. The involvement of NFATC2 in UDP-potentiated IL-12p40 production by BMMs. (**A**) BMMs from WT and *Nfatc2*$^{-/-}$ mice were treated with UDP (30 μM) for 1 h and Df (100 μg/ml) for 6 h. IL-12p40 in supernatants was quantified by ELISA ($n = 8$ from 8 mice, two experiments, except for *Csf2* with $n = 4$ from 4 mice). (**B**) *Il12b*, *Ccl5*, and *Csf2* transcripts of BMMs from +/+ and *P2ry6*$^{fl/fl/Cre/+}$ (Cre/+) mice were measured by qPCR ($n = 6$ from 6 mice, two experiments). Values are means ± SEM. *$p < 0.05$, **$p < 0.01$, ***$p < 0.001$ versus vehicle treatment, by paired *t* test; $^{\#}p < 0.05$, $^{\#\#\#}p < 0.001$, $^{\#\#\#\#}p < 0.0001$ versus +/+ mice, by one-way ANOVA followed by Tukey's multiple comparison test.

decrease in expression of *Il12b* transcript compared with Df-treated WT mice (Fig. 8B). *Ifng* mRNA was strongly induced in CD11c^{-} BAL fluid cells (that include NK cells) from WT mice but was not induced in *Nfatc2*$^{-/-}$ mice. qPCR confirmed the knockdown of the *Nfatc2* transcript (Fig. 8C). Compared with WT controls, *Nfatc2*$^{-/-}$ mice showed increased numbers of BAL fluid total cells and eosinophils on day 16 (Fig. 8D). qPCR revealed significantly greater expression of *Epx* (encoding EPO)

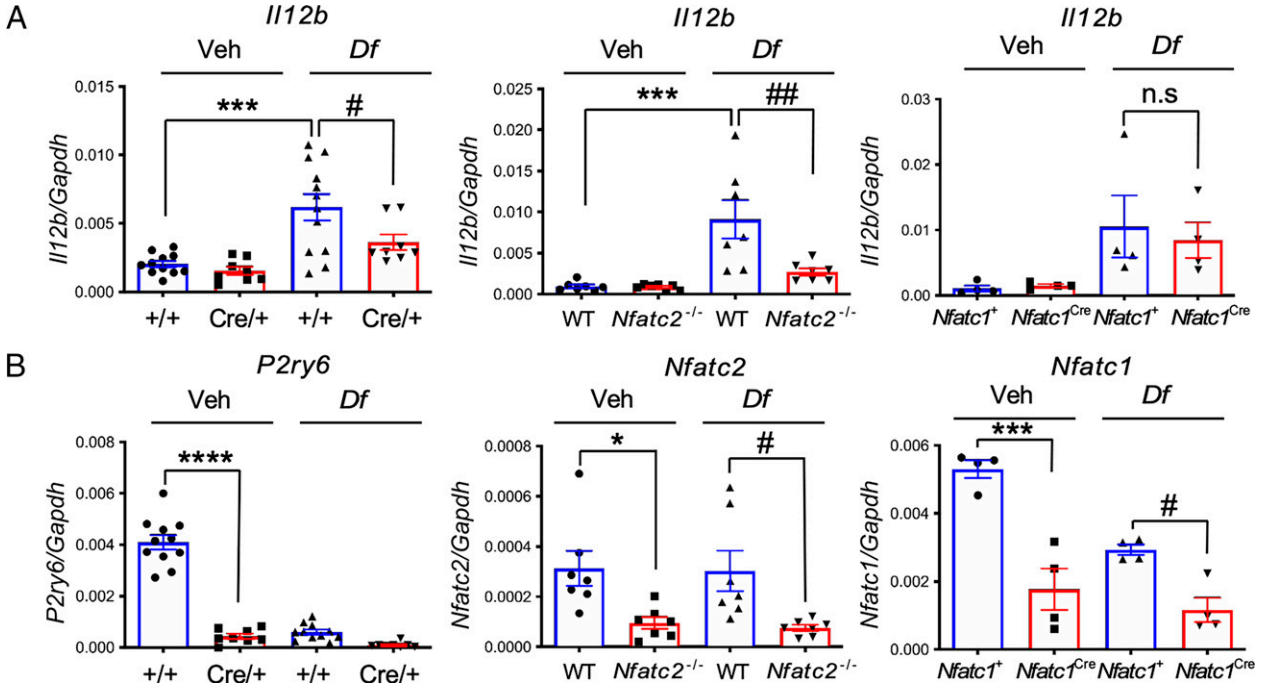

FIGURE 6. The involvement of NFATC2 in Df-induced *Il12b* expression by alveolar macrophages. (**A** and **B**) Alveolar macrophages from +/+ and *P2ry6*$^{fl/fl/Cre/+}$(Cre/+) mice and *Nfatc2*$^{-/-}$ and *Nfatc1*$^{fl/fl/Cre/+}$ (*Nfatc1*^{Cre}) mice were treated with Df (100 μg/ml) for 6 h. *Il12b*, *P2ry6*, *Nfatc2*, and *Nfatc1* transcripts were measured by qPCR ($n = 8$–12 from 8–12 mice from three experiments). Values are means ± SEM. *$p < 0.05$, ***$p < 0.001$, ****$p < 0.001$ versus vehicle treatment; $^{\#}p < 0.05$, $^{\#\#}p < 0.01$, versus +/+ mice, by one-way ANOVA followed by Tukey's multiple comparison test.

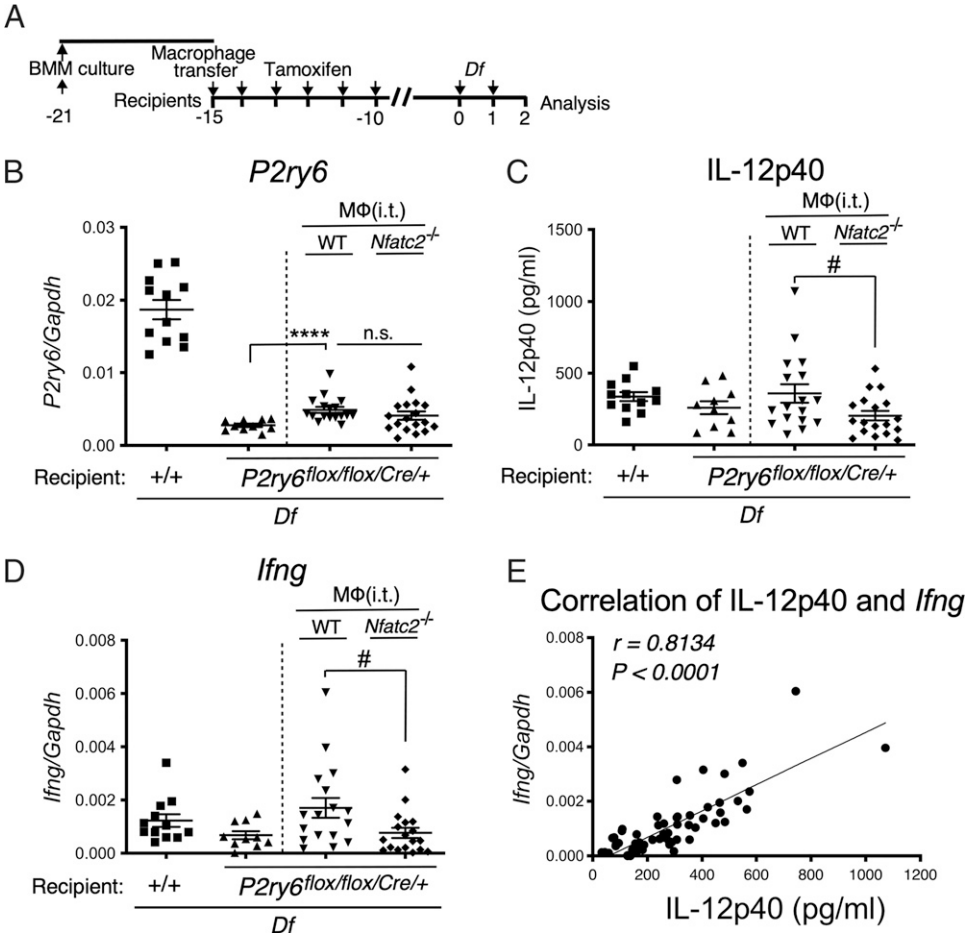

FIGURE 7. Transplantation with WT but not *Nfatc2*$^{-/-}$ macrophages restores Df-induced IL-12p40 production in BAL fluid and *Ifng* transcripts by BAL fluid cells during sensitization of *P2ry6*$^{fl/fl/Cre/+}$ mice. (**A**) BMMs from WT or *Nfatc2*$^{-/-}$ mice were administered intratracheally (i.t.) into *P2ry6*$^{fl/fl/Cre/+}$ mice. (**B**) *P2ry6* transcript in BAL fluid cells of pulmonary macrophage transplantation–treated (PMT-treated) *P2ry6*$^{fl/fl/Cre/+}$ mice on day 2 (17 d after transplantation). (**C**) BAL fluid IL-12p40 from PMT-treated *P2ry6*$^{fl/fl/Cre/+}$ mice on day 2. (**D**) *Ifng* transcripts in BAL fluid cells from mice engrafted with WT or *Nfatc2*$^{-/-}$ macrophages on day 2. (**E**) Correlation between BAL concentration of IL-12p40 and *Ifng* transcripts (n = 10–18 from three experiments). Values are means ± SEM. ****$p <$ 0.0001 versus naive *P2ry6*$^{fl/fl/Cre/+}$ mice; $^{\#}p < 0.05$ versus WT mice, by Mann–Whitney U test.

and *Rnase2* (consistent with the presence of eosinophils) as well as *Il4*, *Il5*, and *Il13* mRNA by BAL fluid cells of Df-treated *Nfatc2*$^{-/-}$ mice than WT controls (Fig. 8E). Levels of IL-5 and IL-13 proteins in BAL fluid were significantly higher in *Nfatc2*$^{-/-}$ mice than in WT controls (Fig. 8F). In contrast, there were no differences between strains in the expression of the goblet cell transcripts Muc5ac by the lungs of Df-treated *Nfatc2*$^{-/-}$ mice than WT controls (Fig. 8G). Serum levels of total IgE significantly rose in the Df-sensitized *Nfatc2*$^{-/-}$, but not WT, mice (Supplemental Fig. 3B).

Discussion

Although adenine nucleotides facilitate the initiation and amplification of T2I, several studies suggest that uracil nucleotides can limit pathologic T2I, particularly at the sensitization phase (21–23, 29, 30). Macrophage/monocyte lineage cells (including alveolar macrophages) strongly express UDP-selective P2Y$_6$ receptors (43). Our previous study demonstrated that P2Y$_6$ signaling on alveolar macrophages and BMMs potentiates IL-12p40 production (along with several cytokines and chemokines) elicited by Df through the pattern recognition receptor dectin 2 (Fig. 1A). This potentiation drives the recruitment of IFN-γ–producing NK cells to the alveolar space, in turn limiting the strength of the pathological T2I-facilitating immune response on subsequent Ag exposure. Because other nucleotides did not potentiate IL-12p40 production (Fig. 1B), we undertook this study to better understand the molecular mechanisms by which P2Y$_6$ elicits this macrophage response.

IL-12p40 can pair with IL-12p35 (*Il12a*) or IL-23p19 (*Il23*) to form IL-12p70 or IL-23, respectively. Both BMM *Il12a* and *Il23* transcripts were induced by Df, but not potentiated by UDP (data not shown). Considering that Df-induced BMM *Il12a* expression level is >100-fold higher than *Il23* (*Il12a*/*Gapdh*, ~0.05; *Il23*/*Gapdh*, 0.0003), IL-12p40 likely mainly couples with IL-12p35. Our previous study demonstrated that intranasal injection of exogenous IL-12p70, but not IL-23, induced IFN-γ production by BAL fluid cells, suggesting the involvement of IL-12p70 rather than IL-23 to potentiate innate immune responses (30).

Among the P2Y receptors, P2Y$_1$, P2Y$_2$, P2Y$_4$, P2Y$_6$, and P2Y$_{11}$ receptors elicit calcium flux through Gαq proteins and PLC, which can activate calcineurin-dependent NFAT transcription factors (16, 44). We suspected the involvement of NFAT family members in P2Y$_6$ receptor–mediated amplification of Df-induced macrophage activation based on the requirement for Gαq (but not Gαi or Gα12/13-RhoA) (Fig. 2), PLC, and calcium signaling, which were dispensable for the baseline production of IL-12p40 elicited by Df alone. These findings were further supported by the abrogation of UDP-induced amplification by calcineurin inhibitors (Fig. 3). We focused on the potential roles of NFATC1, NFATC2, and NFATC3 based on the strong expression levels of their respective transcripts in BMMs (Supplemental Fig. 2A). Notably, the expressions of all three of these NFAT family members (as well as the expression of *P2ry6* transcripts) decreased markedly following stimulation of the BMM with Df (Supplemental Fig. 2B), suggesting a potential mechanism that limits the duration of the amplifying signal.

To facilitate gene expression, NFAT family members require calcium-dependent translocation from the cytoplasm to the nucleus. Accordingly, we found that UDP induced the rapid (10 min) translocation of NFATC2 (and to a lesser extent, NFATC1) in BMMs in a P2Y$_6$ receptor–dependent manner (Fig. 4). As expected, the

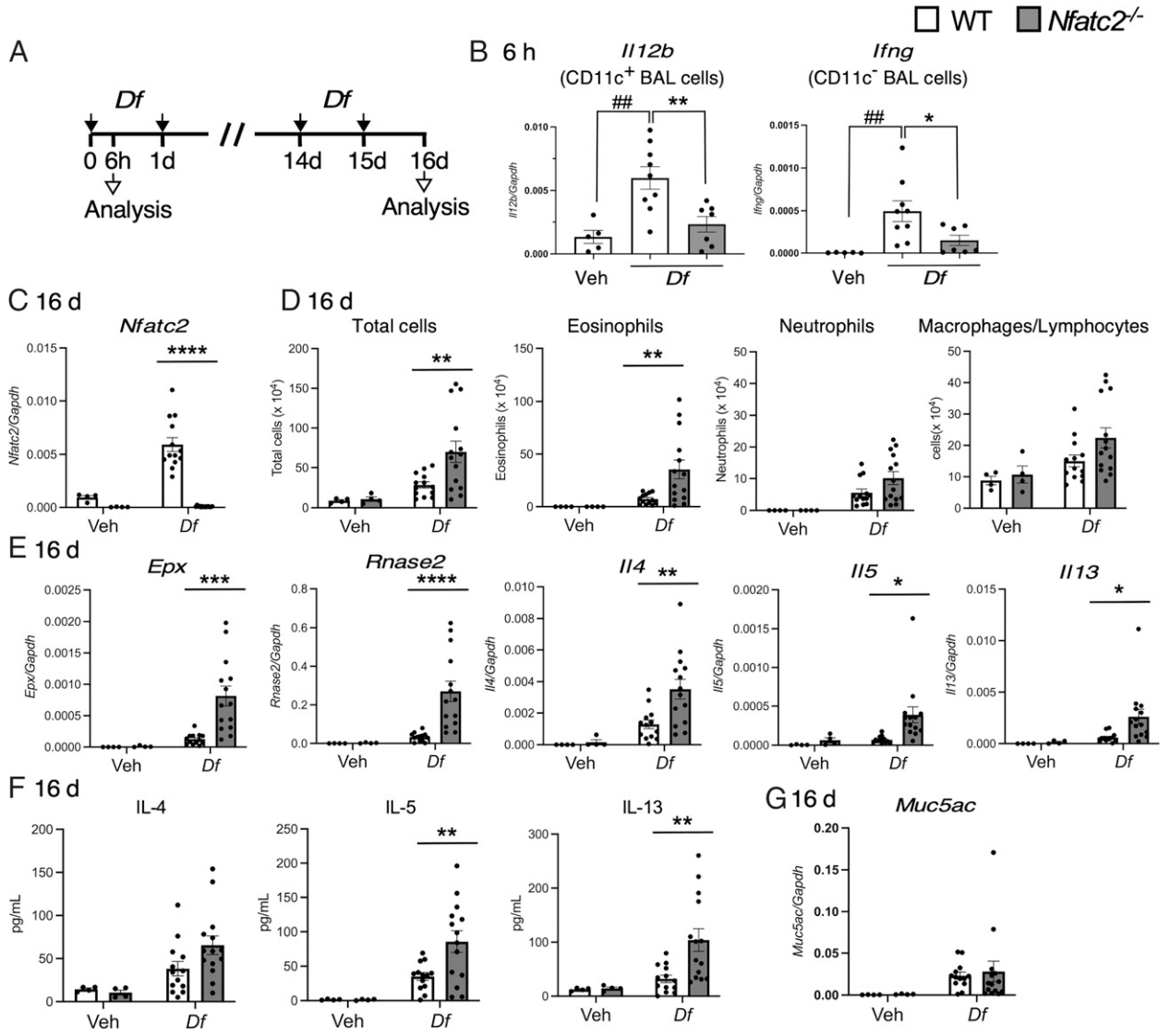

FIGURE 8. Absence of NFATC2 amplifies lung type 2 inflammation in response to Df. (**A**) Protocol to induce allergic airway inflammation on day 16. (**B**) *Il12b* transcripts in alveolar macrophages ($CD11c^+$ BAL fluid cells) and *Ifng* transcripts in $CD11c^-$ BAL fluid cells of WT and *Nfatc2*$^{-/-}$ mice by 6 h after the first sensitization with vehicle ($n = 5$) or Df (WT mice, $n = 7$; *Nfatc2*$^{-/-}$ mice, $n = 9$). Values are means ± SEM. Data are from two experiments. $^{*}p < 0.05$, $^{**}p < 0.01$, $^{\#\#}p < 0.01$, by one-way ANOVA followed by Tukey's multiple comparison test. (**C**) *Nfatc2* transcripts in BAL fluid cells from vehicle ($n = 4$)- or Df ($n = 13$–14)-treated WT (white bars) and *Nfatc2*$^{-/-}$ mice (gray bars) on day 16. (**D**) Total/differential cell counts in BAL fluid of vehicle- or Df-treated WT and *Nfatc2*$^{-/-}$ mice on day 16. (**E**) *Epx* (eosinophil peroxidase), *Rnase2* (consistent with the presence of eosinophils), *Il4*, *Il5*, and *Il13* transcripts in BAL fluid cells from vehicle- or Df-treated WT and *Nfatc2*$^{-/-}$ mice on day 16. (**F**) BAL fluid levels of IL-4, IL-5, and IL-13 in vehicle- or Df-treated WT and *Nfatc2*$^{-/-}$ mice on day 16. (**G**) Lung level of *Muc5ac* in vehicle- or Df-treated WT and *Nfatc2*$^{-/-}$ mice on day 16. Values are means ± SEM. Data are from two experiments. $^{*}p < 0.05$, $^{**}p < 0.01$, $^{****}p < 0.001$, $^{****}p < 0.0001$ versus WT mice, by two-way ANOVA followed by Bonferroni's multiple comparison test.

translocation of NFATC2 induced by UDP was blocked by calcineurin inhibitors. Curiously, NFATC3 did not translocate, even in response to calcium ionophore, suggesting that its regulation and function differ from its orthologs and are distinct from its essential function in T cell–mediated cytokine generation (45). Studies in BMMs from knockout mice confirmed that NFATC2 is essential to the UDP/$P2Y_6$-dependent amplification of IL-12p40 production, as well as the expression of other transcripts (*Ccl5*, *Csf2*) that are targets of this pathway (Fig. 5). Interestingly, ex vivo alveolar macrophages from *P2ry6*$^{fl/fl/Cre/+}$ mice showed decreased Df-induced IL-12p40 production without requiring exogenous UDP priming, suggesting that alveolar macrophages are primed in vivo by endogenous UDP before or during the Df stimulation (Fig. 6A). This in vivo priming of $P2Y_6$ signaling makes it more challenging to evaluate the signaling events downstream of $P2Y_6$ receptors in alveolar macrophages, unlike BMMs. However, the fact that alveolar macrophages harvested from the lungs of *Nfatc2*$^{-/-}$ mice also displayed reduced Df-induced *Il12b* expression is consistent with an ex vivo UDP/$P2Y_6$-dependent priming event that requires NFATC2 to amplify Df-induced production of IL-12p40 (Fig. 6). In contrast, macrophages from *Nfatc1*$^{-/-}$ mice were indistinguishable from WT mice. These observations support the essential and specific nature of NFATC2 as a downstream effector of $P2Y_6$ on macrophages during initial exposure to allergen.

By varying the timing of tamoxifen-induced $P2Y_6$ receptor deletion in *P2ry6*$^{fl/fl/Cre/+}$ mice, we previously demonstrated that the presence of $P2Y_6$ receptor signaling on alveolar macrophages was necessary at the initial exposure to Df to blunt lung T2I after subsequent challenge (30). In this model, the sensitizing dose of Df increased the levels of UDP detected in BAL fluid as early as 3 h.

Although the main source of Df-induced UDP release in vivo has not been identified, the current study suggests that alveolar macrophages release UDP in an autocrine manner to enforce innate immune responses (Fig. 6A). Because UDP is universally stored in cells, it seems likely that other host cells, such as epithelial cells, could release UDP in the same way as well-characterized ATP as DAMPs (4, 22). To determine whether this function required NFATC2, we transferred BMMs from WT and *Nfatc2*$^{-/-}$ mice into naive *P2ry6*$^{fl/fl/Cre/+}$ recipient mice due to the lack of currently available alveolar macrophage–selective cre mice and conditional cre mice to avoid any developmental compensation caused from *Nfatc2* deletion at the developmental stage in vivo (46), and performed intranasal sensitization to Df after 2 wk of engraftment. Remarkably, whereas WT macrophages potentiated Df-induced increases in BAL fluid IL-12p40 protein and *Ifng* expression (reflecting the recruitment and activation of NK cells) (30), *Nfatc2*$^{-/-}$ macrophages did not (Fig. 7). IL-12 and IFN-γ play critical roles in potentiating the innate immune responses, inhibiting allergic inflammation (47–50). Our previous study identified an essential contribution from $P2Y_6$ receptor–regulated IL-12 in driving an early surge in IFN-γ production by NK cells, resulting in the expression of a characteristic IFN-γ–dependent gene signature and consequent suppression of adaptive T2I (30). Using the same model, our current study demonstrates an essential function for macrophage-intrinsic NFATC2 as a component of this pathway (Fig. 7C–E). Indeed, *Nfatc2*$^{-/-}$ mice displayed decreased the alveolar macrophage *Il12b* transcript and $CD11c^{-}$ fraction *Ifng* expression at the sensitization phase and sharply increased numbers of BAL fluid total cells and eosinophils, increased levels of alveolar cell transcripts encoding eosinophil-associated granule products and type 2 cytokines, and BAL fluid type 2 cytokine proteins compared with WT controls in a model of lung T2I elicited by separate sensitization and challenge steps, similar to *P2ry6*$^{fl/fl/Cre/+}$ mice (Fig. 8) (30). Unlike the *P2ry6*$^{fl/fl/Cre/+}$ mice, *Nfatc2*$^{-/-}$ mice showed a higher level of IgE compared with WT mice, implying that NFATC2 expressed by additional cell types also controls features of the subsequent adaptive immune response. For example, NFATC2 in T cells also activates Th1 inflammation, thereby inhibiting T2I (45, 51, 52). Further investigations are needed to determine the actual contributions from alveolar macrophage- and NFATC2-regulated IL-12 and IFN-γ signatures to the T2I using alveolar macrophage–specific *Nfatc2* deleted mice. Collectively, these findings strongly implicate the macrophage-intrinsic function of NFATC2, driven by UDP and the $P2Y_6$ receptor, in the potentiation of the innate IL-12/NK cell/IFN-γ axis that restrains the development of subsequent pathogenetic adaptive type 2 immune responses.

Our findings further strengthen the concept that the UDP/$P2Y_6$ axis on alveolar macrophages limits the consequences of inhaled allergen exposure by limiting pathological type 2 adaptive immune responses, and they implicate a highly specific role for NFATC2 in this process, for the first time, to our knowledge. These findings may carry broader implications for the "fine tuning" of innate immune responses by GPCRs that use canonical Gαq signaling. Recently, two additional Gαq-linked receptors ($CysLT_1R$ and the neuromedin U1 [NMU_1] receptor) were reported to activate NFATC1 and NFATC2 in group 2 innate lymphoid cells, amplifying their production of type 2 cytokines in response to the innate cytokines IL-25 and IL-33 (53, 54). Calcium-driven activation of NFAT family members can drive remodeling of promoters that facilitate gene induction in response to cell stimulation. It seems possible that cooperation between Gαq signaling and NFAT has specialized functions in innate immune cells that permit Gαq-coupled receptors to amplify gene induction initiated by NF-κB–linked receptors, with biological consequences that vary depending on stimulus and context.

Acknowledgments

We thank Anjana Rao and Patrick Hogan for *Nfatc2*$^{-/-}$ mice and Antonios O. Aliprantis for *Nfatc1*$^{fl/fl}$ mice.

Disclosures

The authors have no financial conflicts of interest.

References

1. Holgate, S. T. 2012. Innate and adaptive immune responses in asthma. *Nat. Med.* 18: 673–683.
2. Han, C. Z., I. J. Juncadella, J. M. Kinchen, M. W. Buckley, A. L. Klibanov, K. Dryden, S. Onengut-Gumuscu, U. Erdbrügger, S. D. Turner, Y. M. Shim, et al. 2016. Macrophages redirect phagocytosis by non-professional phagocytes and influence inflammation. *Nature* 539: 570–574.
3. Howitt, M. R., S. Lavoie, M. Michaud, A. M. Blum, S. V. Tran, J. V. Weinstock, C. A. Gallini, K. Redding, R. F. Margolskee, L. C. Osborne, et al. 2016. Tuft cells, taste-chemosensory cells, orchestrate parasite type 2 immunity in the gut. *Science* 351: 1329–1333.
4. Willart, M. A., and B. N. Lambrecht. 2009. The danger within: endogenous danger signals, atopy and asthma. *Clin. Exp. Allergy* 39: 12–19.
5. Ege, M. J., M. Mayer, A. C. Normand, J. Genuneit, W. O. Cookson, C. Braun-Fahrländer, D. Heederik, R. Piarroux, and E. von Mutius; GABRIELA Transregio 22 Study Group. 2011. Exposure to environmental microorganisms and childhood asthma. *N. Engl. J. Med.* 364: 701–709.
6. von Mutius, E., and D. Vercelli. 2010. Farm living: effects on childhood asthma and allergy. *Nat. Rev. Immunol.* 10: 861–868.
7. Schuijs, M. J., M. A. Willart, K. Vergote, D. Gras, K. Deswarte, M. J. Ege, F. B. Madeira, R. Beyaert, G. van Loo, F. Bracher, et al. 2015. Farm dust and endotoxin protect against allergy through A20 induction in lung epithelial cells. *Science* 349: 1106–1110.
8. Bachus, H., K. Kaur, A. M. Papillion, T. T. Marquez-Lago, Z. Yu, A. Ballesteros-Tato, S. Matalon, and B. León. 2019. Impaired tumor-necrosis-factor-α-driven dendritic cell activation limits lipopolysaccharide-induced protection from allergic inflammation in infants. *Immunity* 50: 225–240.e4.
9. Hartl, D., R. Tirouvanziam, J. Laval, C. M. Greene, D. Habiel, L. Sharma, A. O. Yildirim, C. S. Dela Cruz, and C. M. Hogaboam. 2018. Innate immunity of the lung: from basic mechanisms to translational medicine. *J. Innate Immun.* 10: 487–501.
10. Balhara, J., and A. S. Gounni. 2012. The alveolar macrophages in asthma: a double-edged sword. *Mucosal Immunol.* 5: 605–609.
11. Zasłona, Z., S. Przybranowski, C. Wilke, N. van Rooijen, S. Teitz-Tennenbaum, J. J. Osterholzer, J. E. Wilkinson, B. B. Moore, and M. Peters-Golden. 2014. Resident alveolar macrophages suppress, whereas recruited monocytes promote, allergic lung inflammation in murine models of asthma. *J. Immunol.* 193: 4245–4253.
12. Byrne, A. J., M. Weiss, S. A. Mathie, S. A. Walker, H. L. Eames, D. Saliba, C. M. Lloyd, and I. A. Udalova. 2017. A critical role for IRF5 in regulating allergic airway inflammation. *Mucosal Immunol.* 10: 716–726.
13. Di Virgilio, F., A. C. Sarti, and R. Coutinho-Silva. 2020. Purinergic signaling, DAMPs, and inflammation. *Am. J. Physiol. Cell Physiol.* 318: C832–C835.
14. Giuliani, A. L., A. C. Sarti, and F. Di Virgilio. 2019. Extracellular nucleotides and nucleosides as signalling molecules. *Immunol. Lett.* 205: 16–24.
15. Qin, J., G. Zhang, X. Zhang, B. Tan, Z. Lv, M. Liu, H. Ren, M. Qian, and B. Du. 2016. TLR-activated gap junction channels protect mice against bacterial infection through extracellular UDP release. *J. Immunol.* 196: 1790–1798.
16. Erb, L., and G. A. Weisman. 2012. Coupling of P2Y receptors to G proteins and other signaling pathways. *Wiley Interdiscip. Rev. Membr. Transp. Signal.* 1: 789–803.
17. Lau, W. K., A. W. Chow, S. C. Au, and W. H. Ko. 2011. Differential inhibitory effects of $CysLT_1$ receptor antagonists on $P2Y_6$ receptor-mediated signaling and ion transport in human bronchial epithelia. *PLoS One* 6: e22363.
18. Mamedova, L., V. Capra, M. R. Accomazzo, Z. G. Gao, S. Ferrario, M. Fumagalli, M. P. Abbracchio, G. E. Rovati, and K. A. Jacobson. 2005. CysLT1 leukotriene receptor antagonists inhibit the effects of nucleotides acting at P2Y receptors. *Biochem. Pharmacol.* 71: 115–125.
19. Cheng, H., J. A. Leff, R. Amin, B. J. Gertz, M. De Smet, N. Noonan, J. D. Rogers, W. Malbecq, D. Meisner, and G. Somers. 1996. Pharmacokinetics, bioavailability, and safety of montelukast sodium (MK-0476) in healthy males and females. *Pharm. Res.* 13: 445–448.
20. Knorr, B., P. Larson, H. H. Nguyen, S. Holland, T. F. Reiss, P. Chervinsky, K. Blake, C. H. van Nispen, G. Noonan, A. Freeman, et al. 1999. Montelukast dose selection in 6- to 14-year-olds: comparison of single-dose pharmacokinetics in children and adults. *J. Clin. Pharmacol.* 39: 786–793.
21. Idzko, M., H. Hammad, M. van Nimwegen, M. Kool, M. A. Willart, F. Muskens, H. C. Hoogsteden, W. Luttmann, D. Ferrari, F. Di Virgilio, et al. 2007. Extracellular ATP triggers and maintains asthmatic airway inflammation by activating dendritic cells. *Nat. Med.* 13: 913–919.
22. Kouzaki, H., K. Iijima, T. Kobayashi, S. M. O'Grady, and H. Kita. 2011. The danger signal, extracellular ATP, is a sensor for an airborne allergen and triggers IL-33 release and innate Th2-type responses. *J. Immunol.* 186: 4375–4387.
23. Hristova, M., A. Habibovic, C. Veith, Y. M. Janssen-Heininger, A. E. Dixon, M. Geiszt, and A. van der Vliet. 2016. Airway epithelial dual oxidase 1 mediates allergen-induced IL-33 secretion and activation of type 2 immune responses. *J. Allergy Clin. Immunol.* 137: 1545–1556.e11.

24. Kong, X., W. C. Bennett, C. M. Jania, K. D. Chason, Z. German, J. Adouli, S. D. Budney, B. T. Oby, C. van Heusden, E. R. Lazarowski, et al. 2021. Identification of an ATP/P2X7/mast cell pathway mediating ozone-induced bronchial hyperresponsiveness. *JCI Insight* 6: e140207.
25. Jordan, P. M., N. Andreas, M. Groth, P. Wegner, F. Weber, U. Jäger, C. Küchler, O. Werz, E. Serfling, T. Kamradt, et al. 2021. ATP/IL-33-triggered hyperactivation of mast cells results in an amplified production of pro-inflammatory cytokines and eicosanoids. *Immunology* 164: 541–554.
26. Nakamura, Y., T. Sasaki, C. Mochizuki, K. Ishimaru, S. Koizumi, H. Shinmori, K. Suzuki-Inoue, and A. Nakao. 2019. Snake venom rhodocytin induces plasma extravasation via toxin-mediated interactions between platelets and mast cells. *Sci. Rep.* 9: 15958.
27. Werder, R. B., M. A. Ullah, M. M. Rahman, J. Simpson, J. P. Lynch, N. Collinson, S. Rittchen, R. B. Rashid, M. A. A. Sikder, H. Y. Handoko, et al. 2022. Targeting the $P2Y_{13}$ receptor suppresses IL-33 and HMGB1 release and ameliorates experimental asthma. *Am. J. Respir. Crit. Care Med.* 205: 300–312.
28. Myrtek, D., T. Müller, V. Geyer, N. Derr, D. Ferrari, G. Zissel, T. Dürk, S. Sorichter, W. Luttmann, M. Kuepper, et al. 2008. Activation of human alveolar macrophages via P2 receptors: coupling to intracellular Ca^{2+} increases and cytokine secretion. *J. Immunol.* 181: 2181–2188.
29. Giannattasio, G., S. Ohta, J. R. Boyce, W. Xing, B. Balestrieri, and J. A. Boyce. 2011. The purinergic G protein-coupled receptor 6 inhibits effector T cell activation in allergic pulmonary inflammation. *J. Immunol.* 187: 1486–1495.
30. Nagai, J., B. Balestrieri, L. B. Fanning, T. Kyin, H. Cirka, J. Lin, M. Idzko, A. Zech, E. Y. Kim, P. J. Brennan, and J. A. Boyce. 2019. P2Y6 signaling in alveolar macrophages prevents leukotriene-dependent type 2 allergic lung inflammation. *J. Clin. Invest.* 129: 5169–5186.
31. Chetty, A., A. Sharda, R. Warburton, E. O. Weinberg, J. Dong, M. Fang, G. G. Sahagian, T. Chen, C. Xue, J. J. Castellot, et al. 2018. A purinergic P2Y6 receptor agonist prodrug modulates airway inflammation, remodeling, and hyperreactivity in a mouse model of asthma. *J. Asthma Allergy* 11: 159–171.
32. Aliprantis, A. O., Y. Ueki, R. Sulyanto, A. Park, K. S. Sigrist, S. M. Sharma, M. C. Ostrowski, B. R. Olsen, and L. H. Glimcher. 2008. NFATc1 in mice represses osteoprotegerin during osteoclastogenesis and dissociates systemic osteopenia from inflammation in cherubism. *J. Clin. Invest.* 118: 3775–3789.
33. Yona, S., K. W. Kim, Y. Wolf, A. Mildner, D. Varol, M. Breker, D. Strauss-Ayali, S. Viukov, M. Guilliams, A. Misharin, et al. 2013. Fate mapping reveals origins and dynamics of monocytes and tissue macrophages under homeostasis. [Published erratum appears in 2013 *Immunity* 38: 1073–1079.] *Immunity* 38: 79–91.
34. Xanthoudakis, S., J. P. Viola, K. T. Shaw, C. Luo, J. D. Wallace, P. T. Bozza, D. C. Luk, T. Curran, and A. Rao. 1996. An enhanced immune response in mice lacking the transcription factor NFAT1. *Science* 272: 892–895.
35. Suzuki, T., P. Arumugam, T. Sakagami, N. Lachmann, C. Chalk, A. Sallese, S. Abe, C. Trapnell, B. Carey, T. Moritz, et al. 2014. Pulmonary macrophage transplantation therapy. *Nature* 514: 450–454.
36. Inoue, A., F. Raimondi, F. M. N. Kadji, G. Singh, T. Kishi, A. Uwamizu, Y. Ono, Y. Shinjo, S. Ishida, N. Arang, et al. 2019. Illuminating G-protein-coupling selectivity of GPCRs. *Cell* 177: 1933–1947.e25.
37. Takasaki, J., T. Saito, M. Taniguchi, T. Kawasaki, Y. Moritani, K. Hayashi, and M. Kobori. 2004. A novel $G\alpha_{q/11}$-selective inhibitor. *J. Biol. Chem.* 279: 47438–47445.
38. Bair, A. M., P. B. Thippegowda, M. Freichel, N. Cheng, R. D. Ye, S. M. Vogel, Y. Yu, V. Flockerzi, A. B. Malik, and C. Tiruppathi. 2009. Ca^{2+} entry via TRPC channels is necessary for thrombin-induced NF-κB activation in endothelial cells through AMP-activated protein kinase and protein kinase Cδ. *J. Biol. Chem.* 284: 563–574.
39. Rao, A. 2009. Signaling to gene expression: calcium, calcineurin and NFAT. *Nat. Immunol.* 10: 3–5.
40. Communi, D., M. Parmentier, and J. M. Boeynaems. 1996. Cloning, functional expression and tissue distribution of the human P2Y6 receptor. *Biochem. Biophys. Res. Commun.* 222: 303–308.
41. Kingeter, L. M., and X. Lin. 2012. C-type lectin receptor-induced NF-κB activation in innate immune and inflammatory responses. *Cell. Mol. Immunol.* 9: 105–112.
42. Barrett, N. A., O. M. Rahman, J. M. Fernandez, M. W. Parsons, W. Xing, K. F. Austen, and Y. Kanaoka. 2011. Dectin-2 mediates Th2 immunity through the generation of cysteinyl leukotrienes. *J. Exp. Med.* 208: 593–604.
43. Jin, J., V. R. Dasari, F. D. Sistare, and S. P. Kunapuli. 1998. Distribution of P2Y receptor subtypes on haematopoietic cells. *Br. J. Pharmacol.* 123: 789–794.
44. Kim, B., H. K. Jeong, J. H. Kim, S. Y. Lee, I. Jou, and E. H. Joe. 2011. Uridine 5′-diphosphate induces chemokine expression in microglia and astrocytes through activation of the P2Y6 receptor. *J. Immunol.* 186: 3701–3709.
45. Lee, J. U., L. K. Kim, and J. M. Choi. 2018. Revisiting the concept of targeting NFAT to control T cell immunity and autoimmune diseases. *Front. Immunol.* 9: 2747.
46. Gibbings, S. L., S. M. Thomas, S. M. Atif, A. L. McCubbrey, A. N. Desch, T. Danhorn, S. M. Leach, D. L. Bratton, P. M. Henson, W. J. Janssen, and C. V. Jakubzick. 2017. Three unique interstitial macrophages in the murine lung at steady state. *Am. J. Respir. Cell Mol. Biol.* 57: 66–76.
47. Yoshida, M., R. Leigh, K. Matsumoto, J. Wattie, R. Ellis, P. M. O'Byrne, and M. D. Inman. 2002. Effect of interferon-γ on allergic airway responses in interferon-γ-deficient mice. *Am. J. Respir. Crit. Care Med.* 166: 451–456.
48. Kips, J. C., G. J. Brusselle, G. F. Joos, R. A. Peleman, J. H. Tavernier, R. R. Devos, and R. A. Pauwels. 1996. Interleukin-12 inhibits antigen-induced airway hyperresponsiveness in mice. *Am. J. Respir. Crit. Care Med.* 153: 535–539.
49. Zhao, L. L., A. Lindén, M. Sjöstrand, Z. H. Cui, J. Lötvall, and M. Jordana. 2000. IL-12 regulates bone marrow eosinophilia and airway eotaxin levels induced by airway allergen exposure. *Allergy* 55: 749–756.
50. Gavett, S. H., D. J. O'Hearn, X. Li, S. K. Huang, F. D. Finkelman, and M. Wills-Karp. 1995. Interleukin 12 inhibits antigen-induced airway hyperresponsiveness, inflammation, and Th2 cytokine expression in mice. *J. Exp. Med.* 182: 1527–1536.
51. Fonseca, B. P., P. C. Olsen, L. P. Coelho, T. P. Ferreira, H. S. Souza, M. A. Martins, and J. P. Viola. 2009. NFAT1 transcription factor regulates pulmonary allergic inflammation and airway responsiveness. *Am. J. Respir. Cell Mol. Biol.* 40: 66–75.
52. Kiani, A., J. P. Viola, A. H. Lichtman, and A. Rao. 1997. Down-regulation of IL-4 gene transcription and control of Th2 cell differentiation by a mechanism involving NFAT1. *Immunity* 7: 849–860.
53. Cardoso, V., J. Chesné, H. Ribeiro, B. García-Cassani, T. Carvalho, T. Bouchery, K. Shah, N. L. Barbosa-Morais, N. Harris, and H. Veiga-Fernandes. 2017. Neuronal regulation of type 2 innate lymphoid cells via neuromedin U. *Nature* 549: 277–281.
54. von Moltke, J., C. E. O'Leary, N. A. Barrett, Y. Kanaoka, K. F. Austen, and R. M. Locksley. 2017. Leukotrienes provide an NFAT-dependent signal that synergizes with IL-33 to activate ILC2s. *J. Exp. Med.* 214: 27–37.